Sensors & Actuators: B. Chemical 444 (2025) 138480

Contents lists available at ScienceDirect

Sensors and Actuators: B. Chemical

journal homepage: www.elsevier.com/locate/snb

Engineering a multifunctional hybrid polymer-hydrogel nanocomposite for high-sensitivity, anti-fouling electrochemical immunodetection in early cancer diagnosis

Verónica Serafín [a,1], Andrea Cabrero-Martín [a,1], Sara Santiago [a,*], Ceren Yildiz [a,b], María Pedrero [a], Ana Montero-Calle [c], Zehra Yazan [b], Dilek Eskiköy Bayraktepe [b], José M. Pingarrón [a], Rodrigo Barderas [c,d], Susana Campuzano [a,d,**]

[a] Departamento de Química Analítica, Facultad de CC. Químicas, Universidad Complutense de Madrid, Pza. de las Ciencias 2, Madrid 28040, Spain
[b] Ankara University, Faculty of Science Department of Chemistry, Ankara 06560, Turkey
[c] Chronic Disease Programme, UFIEC, Institute of Health Carlos III, Majadahonda, Madrid 28220, Spain
[d] CIBER of Frailty and Healthy Aging (CIBERFES), Instituto de Salud Carlos III, Madrid 28046, Spain

ARTICLE INFO

Keywords:
Hybrid polymer-hydrogel nanocomposite
Electrochemical immunosensor
Antifouling properties
Human endostatin
Colorectal cancer
Plasma

ABSTRACT

This work introduces a novel dual-component electrode modifier comprising gold nanoparticles (AuNPs) and a hydrated form of the poly(3,4-ethylenedioxythiophene) (hPEDOT) conducting polymer to enhance biomolecule immobilization and signal amplification in electrochemical immunosensing. The thiophene–AuNP interaction promotes electropolymerization, forming a citrate-doped matrix with carboxyl groups that enable covalent, oriented antibody anchoring. Moreover, the hydration of the polymeric scaffold enhances the biocompatibility and anti-fouling properties of the sensing interface. This multifunctional polymer–hydrogel nanocomposite was used to develop a disposable sandwich-type electrochemical immunoplatform for the determination of human endostatin (HE), a biomarker of colorectal cancer (CRC). The immunoplatform achieved a detection limit of 0.04 ng mL^{-1} and distinguished not only healthy individuals from early-stage CRC patients but also from those with premalignant colorectal lesions. These findings underscore the potential of this new multifunctional hybrid nanocomposite to improve the performance of electrochemical immunosensing, which is crucial for timely cancer diagnosis and intervention.

1. Introduction

Organic conducting polymers (CPs) have a high interest as bio-interfaces in bioelectronics and medical applications. Due to their tuneable conductivity allowing free movement of π-electrons along their structure, light weight, low manufacturing cost, robustness, easy fabrication, and modification with biorecognition components, they are used in the design of sensors and biosensors with applications in medical diagnostics, environmental monitoring, and food safety [1–3]. These biointerfaces may be incorporated into sensing platforms via electrochemical polymerization and hydrogel coating and to enhance their conductivity they are doped with either metal nanoparticles, metal oxides, and carbonaceous chemicals [1]. Poly (3,4-ethylenedioxythiophene) (PEDOT), a biocompatible conducting polymer, with low oxidation potential, easy functionalization, soft nature, and film-forming ability [2,4–6], has attracted great attention for the fabrication of conducting polymeric hydrogels (CPHs) [7] as well as of nanocomposites that combine the electrocatalytic properties of the CP with the favoured electron transfer and high surface area of nanomaterials [2,4]. PEDOT has been doped with anionic molecules and with other polymers to increase its conductivity as well as with anions added to EDOT solutions to start the polymerization process [8]. This is the case of citrate giving rise to negatively charged carboxylic acid groups functionalized PEDOT [9] that allows the stabilization of AuNPs due to

* Corresponding author.
** Corresponding author at: Departamento de Química Analítica, Facultad de CC. Químicas, Universidad Complutense de Madrid, Pza. de las Ciencias 2, Madrid 28040, Spain.
E-mail addresses: ssanti02@ucm.es (S. Santiago), susanacr@quim.ucm.es (S. Campuzano).
[1] These authors contributed equally to this work and shared first authorship

https://doi.org/10.1016/j.snb.2025.138480
Received 8 July 2025; Received in revised form 4 August 2025; Accepted 5 August 2025
Available online 6 August 2025

their high affinity to the sulfur atom in the thiophene rings [10] forming PEDOT-based nanocomposites with enhanced electrochemical responses [11]. Moreover, CPHs combine the electroactivity provided by CPs and the ionic conductivity provided by hydrogels aqueous medium, giving rise to biocompatible anti-fouling interfaces between electrodes and electrolytes whose three-dimensional microstructure facilitates the transport of ions, and molecules [7,12].

The production of biocompatible stable interfaces between electrode surfaces and the solutions to be analyzed may involve the use of new varieties of CPs or the modification of the CPs chemical structure. With all this in mind a novel nanostructured hybrid material combining the hydrated form of poly(3,4-ethylenedioxythiophene) (hPEDOT) and gold nanoparticles (AuNPs) is developed in this work to be used in electrochemical immunosensing. The hPEDOT matrix was synthesized in the presence of citrate ions and $LiClO_4$ and exhibits a high density of surface-exposed carboxylic acid groups [9], allowing an efficient covalent immobilization of antibodies. The integration of AuNPs enables a controlled nanostructuration of the conducting polymer, leading to enhanced electrical conductivity and electron transfer capabilities. This novel synergistic architecture results in a stable, antifouling interface which was built on screen-printed carbon electrodes (SPCEs) and allowed minimization of non-specific adsorption and supported reliable biorecognition [13]. Its analytical performance was checked by the development of a sandwich-type amperometric immunosensor for the simple and rapid determination in serum of human endostatin (HE), to detect both precancerous colorectal lesions and colorectal cancer (CRC). HE is a biomarker associated with tumor angiogenesis [14] and CRC development and progression with reported cut-off values of 172 ng mL^{-1} [15] and 67.8 ng mL^{-1} [14] in serum and plasma, respectively, to discriminate healthy individuals from CRC patients. It is important to highlight that literature includes some electrochemical immunosensors that exploit the use of nanocomposites also comprising PEDOT and AuNPs as electrode modifier (SPCEs [5,16] and steel mesh [17]). However, all these reported immunosensors used direct and label-free immunoassays involving impedimetric and/or voltammetric detection and nanocomposites based on PEDOT and not hPEDOT. In all cases, the electrode was first modified with the CP and then with the AuNPs on which the antibody was immobilized by chemisorption of its amine groups. Thus, the main innovations of the strategy reported in this work are the arrangement of the nanocomposite, the use of hPEDOT, further functionalized with -COOH groups for the covalent immobilization of the capture antibody, and its exploration in a sandwich immunoassay format in connection with amperometric transduction.

2. Materials and methods

Instrumentation and electrochemical setup, and Reagents and solutions, are detailed in the Supporting Information.

2.1. Experimental procedures

2.1.1. Electrodeposition of AuNPs on SPCEs

The electrodeposition of AuNPs on the SPCE working carbon electrode was carried out according to the method described by Carralero et al. [18]. The electrode was immersed into a 2.5 mM $HAuCl_4$ solution, prepared by accurately weighing the required amount of $HAuCl_4$ and dissolving it in filtered Milli-Q purified water. A potential of − 0.20 V was applied for 60 s. Following electrodeposition, the electrode was rinsed with deionized water and dried under a nitrogen stream.

2.1.2. EDOT electropolymerization and PEDOT hydration

PEDOT polymer electrodeposition on the AuNPs/SPCE was performed according to the method outlined by Promsuwan et al. [19], with some modification. In brief, the AuNPs/SPCE was immersed into an electrochemical cell containing 1.6 mL of a mixture solution of 5 mM EDOT monomer, 30 mM sodium citrate, and 20 mM $LiClO_4$ prepared in 0.1 M H_2SO_4 (previously sonicated to ensure suspension uniformity) [9,20].

Then, a constant oxidation potential of + 1.10 V was applied for 30 s to facilitate the formation of PEDOT/AuNPs/SPCE. Thereafter, the electrode was rinsed with deionized water, and 40 μL of PBS were added to the electrode surface [21]. Next, the assembly in PBS was maintained in a humid environment at 4 °C overnight to promote hydration of the polymer film, resulting in the formation of the polymeric hydrogel on the electrode surface (hPEDOT/AuNPs/SPCE).

2.1.3. Preparation of the immunoplatform for the determination of HE

A sandwich-type immunoplatform for the determination of HE was constructed on the hPEDOT/AuNPs/SPCEs. The process began with the activation of free carboxyl groups on the hPEDOT/AuNPs/SPCE by dropping 10 μL of a 0.4/0.1 M EDC/sulfo-NHS solution prepared in MES buffer on the WE surface. The activation process was conducted under dark, humid conditions and room temperature for 30 min.

Thereafter, the HE specific capture antibody (cAb) was covalently immobilized onto the modified WE surface through amide bond formation between the activated carboxyl groups of the hPEDOT and the amino groups of the cAb. The immobilization was carried out by adding 5 μL of a 50 μg mL^{-1} cAb solution to the activated hPEDOT/AuNPs/SPCEs in a humid chamber for an additional 30 min-time period.

Next, to minimize nonspecific adsorptions, unreacted activated carboxyl groups were blocked with 10 μL of a 0.5 % BSA solution for 15 min in a humid chamber. The electrode was then incubated for 30 min in 5 μL of a solution containing the standard analyte, facilitating the capture of the target protein via specific antibody-antigen interaction.

Subsequently, the electrode underwent a 30-min incubation step in a humid environment with 5 μL of a 0.25 μg mL^{-1} biotin-conjugated specific detection antibody (btn-dAb) solution, thus implementing the sandwich immunoassay configuration. Finally, the btn-dAb was linked to a commercial Strep-HRP complex by adding 5 μL of a 0.5 μg mL^{-1} Strep-HRP solution in a humid chamber for 60 min.

Between incubation periods, the modified SPCEs were rinsed either with MES buffer solution or with PBS (before and after the blocking step, respectively).

For comparative purposes, immunoplatforms were also constructed following the same protocol but immobilizing the cAb covalently on *p*-ABA/SPCEs as previously reported [22] instead of on hPEDOT/AuNPs/SPCEs.

2.1.4. Amperometric detection and electrochemical analysis

The quantification of HE was performed by amperometry in stirred solutions, exploiting the reactions cascade initiated by the enzymatic reduction of H_2O_2 by Strep-HRP mediated by HQ. To do that, electrodes modified with the immune complexes were immersed into a measurement cell containing 10 mL of 50 mM PB at pH 6.0 and adding 100 μL of freshly prepared 0.1 M HQ solution. Amperometric measurements were conducted in a continuously stirred solution, by applying a constant potential of − 0.20 V relative to the SPCE Ag *pseudo*-reference electrode. Once the background current stabilized, 50 μL of a 0.1 M H_2O_2 solution were added to the cell, and the resulting change in the cathodic current was recorded until reaching the steady state (approximately 50 s). The observed cathodic current variation (measured as the difference between the value of the stabilized current after and before the addition of H_2O_2 in absolute value and referred to in the text as Δi_c) was directly proportional to the concentration of the target antigen according to the assay format used [23]. Furthermore, the Δi_c value measured with platforms prepared without cAb was subtracted from the Δi_c value obtained with platforms prepared in the presence of cAb for each antigen concentration.

The stepwise construction of the immunoplatform was characterized by CV and EIS in a 5 mM $[Fe(CN)_6]^{3-/4-}$ solution in 0.1 M KCl. Regarding CV, the potential range was scanned from − 0.30 to + 0.70 V

at a scan rate of 50 mV s^{-1}. EIS measurements were conducted under open-circuit conditions, employing a sinusoidal excitation amplitude of 10 mV (RMS) across a frequency spectrum ranging from 0.04 Hz to 1×10^5 Hz. The automatic analyzer was calibrated to achieve a standard deviation of 0.001 % for the I (jω) correlator output, with a cutoff time set at 100 s. Data acquisition was performed at a rate of 10 points per decade throughout the specified frequency range to ensure high-resolution data.

Furthermore, the effective electrode area was determined by CV in a 5 mM $[Fe(CN)_6]^{3-/4-}$ solution in 0.1 M KCl at different scan rates. According to the Randles-Sevcik equation for a diffusion-controlled system, the peak current exhibits a linear relationship with the square root of the scan rate. The effective electrode area was determined from the slope of this regression plot after the electrodeposition of AuNPs, the electropolymerization of EDOT and its hydration (hPEDOT), using the known diffusion constants of the $[Fe(CN)_6]^{3-/4-}$ redox system, its concentration, and the number of electrons involved in the electron transfer process [24].

2.1.5. Analysis of plasma samples in CRC scenarios

Plasma samples were obtained from the Hospital Clínico San Carlos from a cohort comprising healthy individuals, patients with colorectal premalignant lesions (low- and high-grade colorectal adenomas), and CRC stage I (CRC (I)) diagnosed individuals. Ethical approval for the study was granted by the relevant Ethical Review Boards of the Hospital Clínico San Carlos and the Instituto de Salud Carlos III for the identification and validation of CRC biomarkers (CEI PI 13_2020-v2 and CEI PI 90_2023). Prior to analysis, all samples were stored at − 80 °C, according to ethical guidelines and regulations governing the handling of biological specimens and experimental procedures. Written informed consent was obtained from all participants.

Upon confirming the absence of matrix effects in plasma samples, which were 1:200 diluted, amperometric measurements were carried out by interpolation of the obtained current signals into a pre-established calibration curve for HE standards in buffered solutions.

Additionally, Receiver Operating Characteristic (ROC) curves were generated using R software (version 3.6.2), leveraging the 'pROC' package to evaluate the diagnostic capabilities of the immunosensor to discriminate the indicated samples.

3. Results and discussion

In the pursuit of more efficient and reliable biosensing techniques, this study introduces an innovative approach to electrode modification. By electrochemically functionalizing SPCEs with AuNPs and conductive hydrated PEDOT, we developed, characterized, and applied a bio-platform with improved electron transfer and sensitivity also showing anti-fouling properties (Fig. 1).

This multipurpose engineered electrode modifier integrates carboxylic functional groups, allowing the robust covalent immobilization of the cAb through amide coupling to ensure efficient target recognition. In addition, enzyme-labeled sandwich-type immunocomplexes were formed using a biotinylated detection antibody (btn-dAb) and the enzyme tracer (Strep-HRP). This configuration enables the amperometric quantification of HE via the HQ/H_2O_2 system.

3.1. Electrode surface modification and characterization

The working electrode surface modification was performed in two sequential steps:

i) Potentiostatic electrodeposition of AuNPs on SPCE. A constant potential of − 0.20 V (vs. Ag *pseudo*-reference electrode) was applied for 30 s using a 2.5 mM $HAuCl_4$ aqueous solution, resulting in a uniform of AuNPs distribution. The total charge transferred during the electrodeposition was 3.3 mC, corresponding to a current density of 30.0 mC cm^{-2} and an estimated surface density of 3.4×10^{12} AuNPs cm^{-2}. This was calculated assuming compact 8 nm spherical nanoparticles (from SEM), using gold's bulk density (19.32 g cm^{-3}) and atomic weight (196.97g mol^{-1}).

ii) Oriented-assisted electropolymerization of EDOT on the AuNPs/SPCE. The thiophene moiety of the EDOT monomer was pre-oriented on the SPCE surface through π-metal and S–Au interactions with the electrodeposited AuNPs. Electropolymerization was carried out using an aqueous solution containing 5 mM EDOT, 20 mM $LiClO_4$, and 30 mM sodium citrate in 0.1 M H_2SO_4. $LiClO_4$ and citrate acted as both supporting electrolyte and dopant (counter-ion to neutralize EDOT positive charges during oxidative electropolymerization), while citrate also enabled the incorporation of carboxylate groups into the PEDOT interface for enhanced functionalization [9,19]. A total charge of 1.4 mC was applied (current density: 12.7 mC cm^{-2}), leading to 18.2 μg cm^{-2} PEDOT

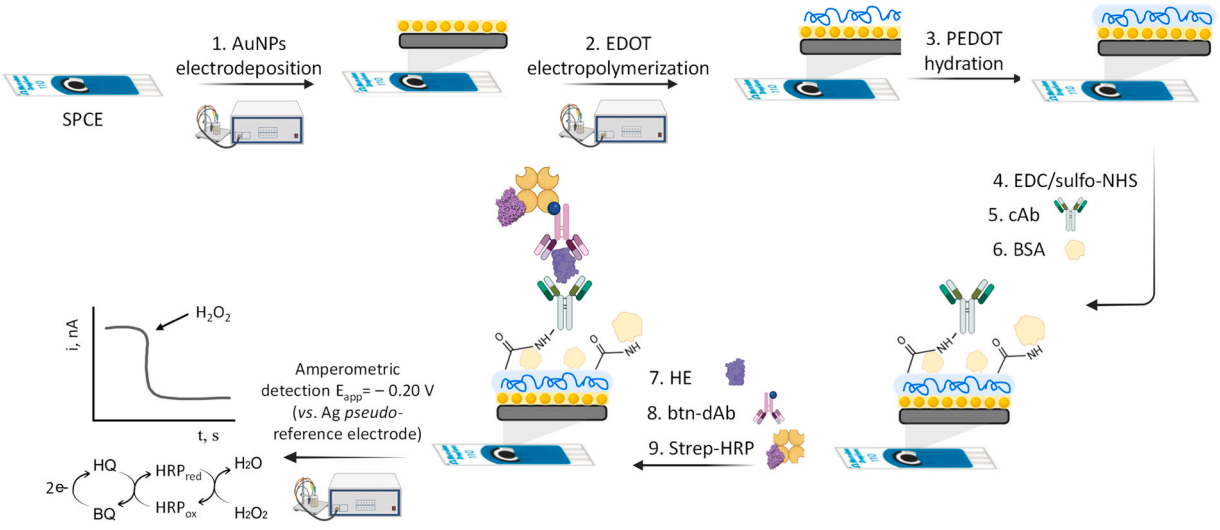

Fig. 1. Schematic representation of the step-by-step immunoplatform preparation and amperometric transduction using the HRP/H_2O_2/HQ system. Created in BioRender. Campuzano Ruiz, S. (2025) https://BioRender.com/uatal34. AuNPs: Gold nanoparticles; BQ: Benzoquinone; BSA: Bovine Serum Albumin; btn-dAb: biotinylated detection antibody; cAb: capture antibody; EDC: N-(3-dimethylaminopropyl)-N′-ethylcarbodiimide; EDOT: 3,4-ethylenedioxythiophene; HE: Human Endostatin; HQ: hydroquinone; PEDOT: poly(3,4-ethylenedioxythiophene); SPCE: Screen-printed carbon electrode; Strep-HRP: streptavidin-peroxidase; sulfo-NHS: N-hydroxysulfosuccinimide.

deposition. Subsequent treatment in aqueous medium promoted PEDOT hydrogel (hPEDOT) formation, improving biocompatibility, stability, and antifouling properties—key for electrochemical biosensor applications [13,21].

To confirm the presence of AuNPs, electrochemical characterization was performed using CV in a 0.1 M H_2SO_4 solution, scanning the potential from 0.00 V to + 1.30 V at a scan rate of 50 mV s^{-1} (Fig. 2**a**). The CV profile of the AuNPs-modified electrode (AuNPs/SPCE) exhibited the characteristic electrochemical behavior of gold in acidic media, with an anodic peak at + 1.16 V, corresponding to gold oxide formation, and a cathodic peak at + 0.45 V, indicating the reduction of this oxide back to metallic gold [25]. As can be seen, the presence of the hPEDOT layer significantly shields both the anodic and cathodic peaks associated with oxidation and reduction of AuNPs. The observed increase in capacitive current is attributed to an enhanced effective electrode surface area resulting from the formation of a more porous structure. Notably, no distinct oxidation or reduction peaks were observed during the potential sweep, since hPEDOT is a conducting polymer with a delocalized electronic structure and a seamless distribution of energy states. This leads to broad, featureless redox behavior, in contrast to the sharp, distinct peaks typically associated with discrete molecules [26]. A high increase in faradaic current is observed at potentials larger than + 0.90 V. This relatively high oxidation potential is attributed to the oxidized form of hPEDOT due to the well-doped polymer with counter anions, which shift the redox processes to higher potentials. These results confirm the successful polymerization of carboxylic acid-doped hPEDOT on the AuNPs/SPCE.

Further characterization of SPCEs modified with AuNPs and (h)PEDOT was performed by CV and EIS in a 5 mM $[Fe(CN)_6]^{3-/4-}$ solution in 0.1 M KCl as redox probe (Fig. 2**b** and **c**). Impedance data were presented as Nyquist plots and analyzed using the Randles circuit (see Table 1).

As expected, CV showed a smaller separation between the redox probe anodic and cathodic peaks compared to the bare electrode upon AuNPs electrodeposition due to an enhanced surface conductivity, and an accelerated electron transfer at the electrode interface. Upon electrodeposition of PEDOT or hPEDOT, either directly onto the SPCE ((h)PEDOT/SPCE) or the AuNPs-modified electrode ((h)PEDOT/AuNPs/SPCE), the peak separation still decreased, and the peak currents increased. This behavior is attributed to the porous structure of (h)PEDOT, which increases the electrochemically active surface area, promoting more efficient diffusion of $[Fe(CN)_6]^{3-/4-}$ ions near the electrode surface [27]. In contrast, no significant differences in conductivity were observed between PEDOT and its hydrated form (hPEDOT), as the conductive properties of the material are primarily governed by the intrinsic characteristics of the electrogenerated polymer.

Table 1
R_{CT} values for all tested surfaces in Fig. 2**c**).

Tested Surfaces	R_{CT} values, Ω
SPCE	1838
AuNPs/SPCE	330
PEDOT/SPCE	173
hPEDOT/SPCE	169
PEDOT/AuNPs/SPCE	135
hPEDOT/AuNPs/SPCE	136

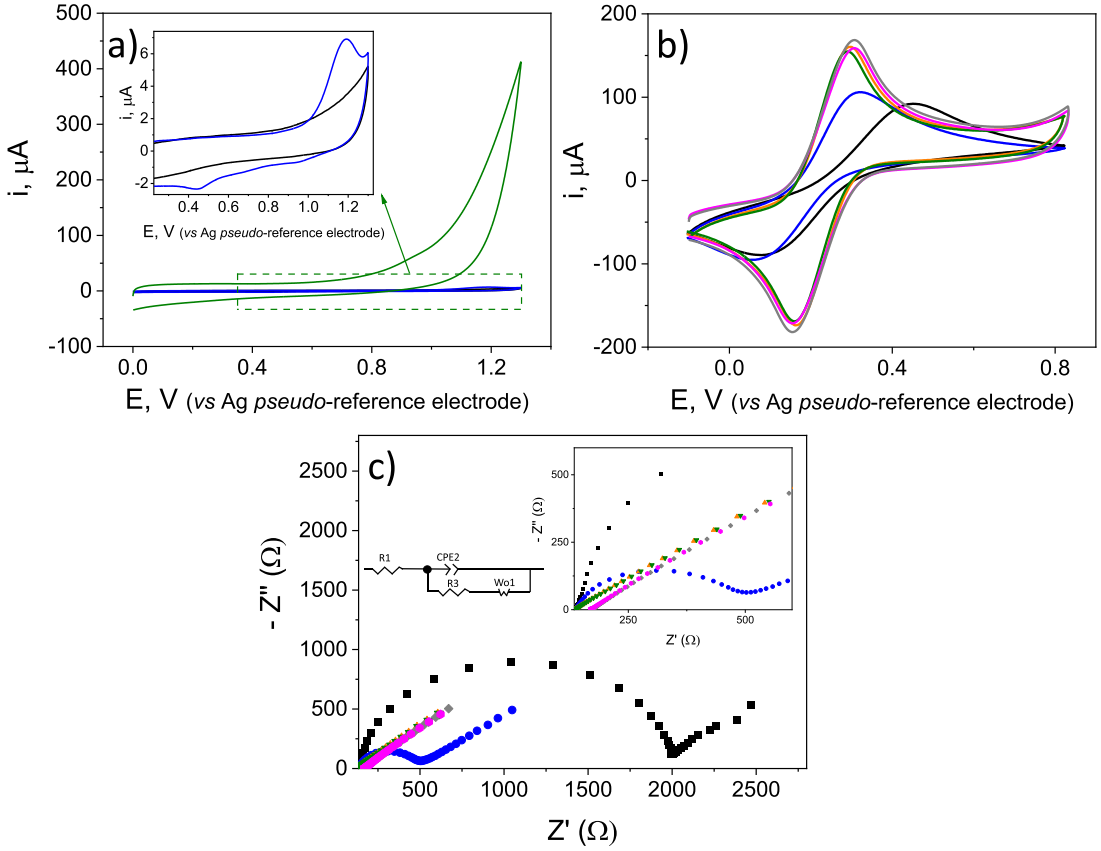

Fig. 2. a) Cyclic voltammograms recorded in 0.1 M H_2SO_4 (from 0.00 V to + 1.30 V;scan rate: 50 mV s^{-1}) with SPCE (black); AuNPs/SPCE (blue); and hPEDOT/AuNPs/SPCE (green). b) Cyclic voltammograms (from − 0.10 V to + 0.80 V; scan rate of 50 mV s^{-1}), c) Nyquist plots (frequency range: 10^5 – 0.04 Hz; amplitude: 0.01 V; applied potential: 0 V) obtained in the presence of 5 mM $[Fe(CN)_6]^{3-/4-}$ redox probe in 0.1 M KCl with SPCE (black), AuNPs/SPCE (blue), PEDOT/SPCE (grey), hPEDOT/SPCE (pink), PEDOT/AuNPs/SPCE (orange), and hPEDOT/AuNPs/SPCE (green). EIS experimental data were fitted to the Randles equivalent circuit inserted in panel.

Consistent with the CV behavior, the EIS Nyquist plots revealed that the modification of the SPCE with AuNPs significantly reduced the charge transfer resistance (R_{CT}) from 1838 Ω to 330 Ω (Fig. 2**d**). This marked decrease highlights the conductive properties of AuNPs, which facilitate electron transfer at the electrode interface. For electrodes modified with both PEDOT and hPEDOT, the EIS plots exhibited a nearly linear region, indicating that the faradaic process of the $[Fe(CN)_6]^{3-/4-}$ redox couple is diffusion-controlled across the frequency range tested. This behavior confirms the formation of a highly conductive surface, demonstrating the suitability of these materials for advanced electrochemical sensing applications.

To determine the effective surface area of the modified electrodes, CV was conducted in a 5 mM $[Fe(CN)_6]^{3-/4-}$ solution in 0.1 M KCl at various scan rates (Fig. S1 in the Supplementary material). Using the Randles-Sevick equation for diffusion-controlled processes, the effective surface area was calculated from the slope of the linear relationship between the anodic peak current and the square root of the scan rate. The diffusion coefficient used was 7.6×10^{-6} cm^2 s^{-1}.

The functionalization of the electrode with AuNPs, PEDOT, and hPEDOT resulted in a progressive increase of the electrochemical active area compared to the bare SPCE (Table S1 in the Supplementary material). The electrodeposition of AuNPs provided nanoscale roughness to the electrode surface, effectively increasing the electrochemical active area by 15 % and acting as spatial orientators for the (h)PEDOT chains during electropolymerization. The electropolymerization of PEDOT, both directly on bare SPCE and on AuNPs, formed a porous and conductive three-dimensional network on the electrode surface, further increasing the active area by 34 %. This structure not only improved the immobilization of biomolecules but also enhanced the conductivity of electrodes. Notably, hPEDOT exhibited the most significant enhancement, with a 53 % increase in the electrochemical active area. The hydration process expanded the polymer matrix, creating a porous and biocompatible structure. This increased surface area maximized the availability of binding sites for biomolecules and provided a stable environment for antigen-antibody complexes. Moreover, the hydrated network facilitated efficient ion and electron transport, further boosting the electrochemical signal. The progressive increase in the active area directly translated into improved sensitivity of the immunoplatform.

AFM imaging confirmed a significant increase in nanoscale roughness, supporting the hypothesis of an enhanced effective electrode area. The average roughness (Ra), defined as the arithmetic mean of the absolute deviations of the surface profile from the mean line over a measured length, exhibited a notable rise in surface irregularity following polymerization. Specifically, Ra increased from (17 ± 4) nm for bare SPCEs to (22 ± 3) nm for PEDOT/AuNPs/SPCEs. More prominently, after polymer hydration (hPEDOT/AuNPs/SPCEs), Ra further increased to (38 ± 3) nm (Fig. S2 in the Supplementary material). This increase is attributed to the swelling effect of the hydrogel as water molecules are absorbed into the polymer network. The incorporation of water induces nanoscale expansion, consistent with the hydrogel formation mechanism, while the resulting increased roughness may further enhance biocompatibility by creating a hydrated microenvironment that supports biomolecular interactions [28].

Surface morphology and compositional characteristics of nanostructured electrode surfaces were investigated by SEM and EDX (Fig. 3). Although SEM images (Fig. 3**a**) did not reveal any significant morphological changes after the electrodeposition of AuNPs, a film formation on the electrode surface was observed at the microscale after the electropolymerization of (h)PEDOT. Nevertheless, backscattered electron imaging provided sufficient contrast to identify the electrodeposited AuNPs, which appeared uniformly distributed as bright white spots against the darker background of the polymer and graphite substrate (Fig. 3**b**). These observations confirm the successful deposition of AuNPs onto the electrode surface. EDX analysis further validated these

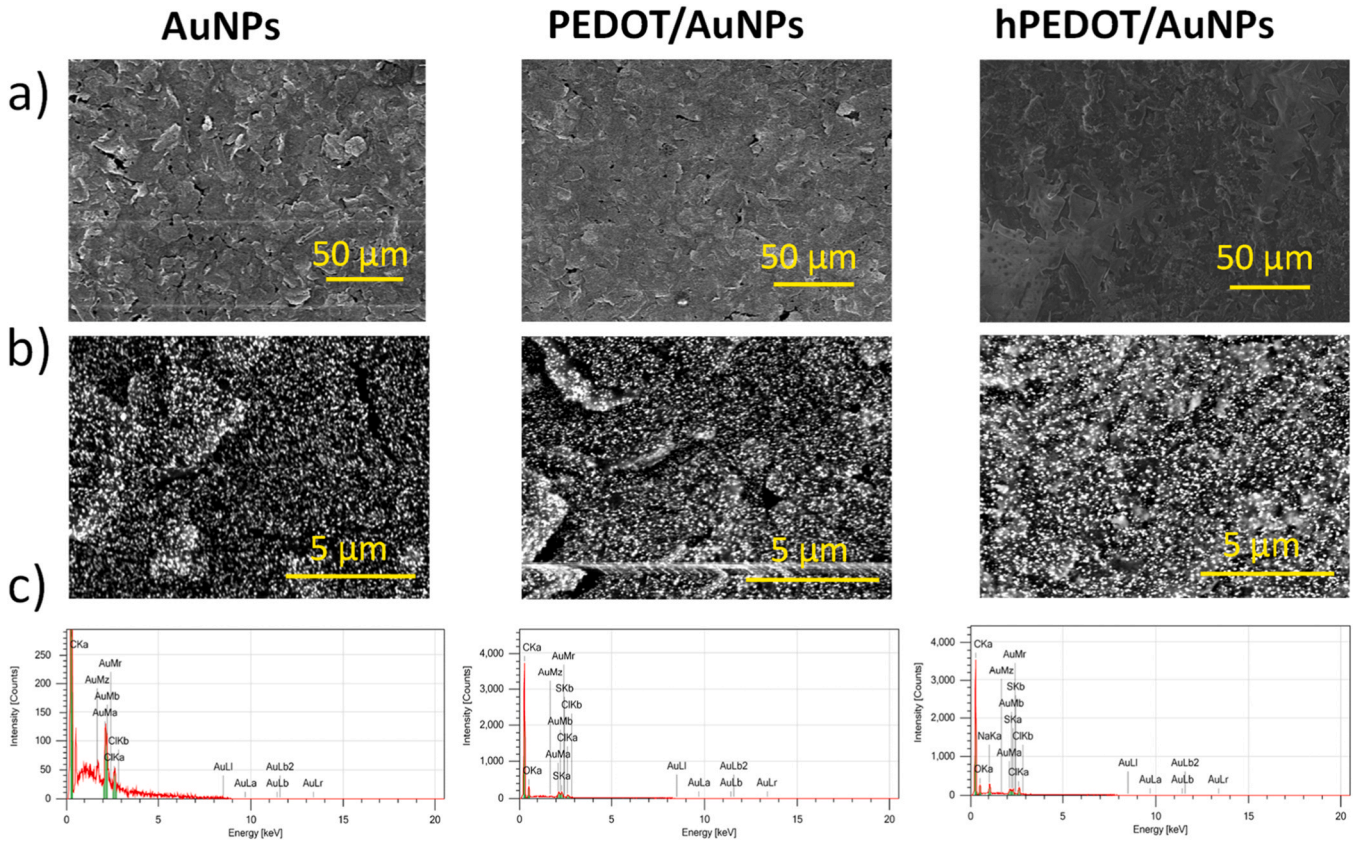

Fig. 3. SEM analysis: a) secondary electron images, b) backscattered electron images; and c) EDX spectra of SPCEs modified with AuNPs, PEDOT/AuNPs, and hPEDOT/AuNPs.

findings by detecting the presence of gold and sulfur, confirming the presence of both AuNPs and (h)PEDOT (Fig. 3**c**).

Cross-sectional imaging (Fig. S3 in the Supplementary material) revealed a clear difference in layer thickness between hydrated and non-hydrated configurations. PEDOT/AuNPs/SPCEs exhibited a total electrode thickness (including the carbon electrode) of 13.3 μm, while hPEDOT/AuNPs/SPCEs reached 20.8 μm. The observed increase in thickness for hPEDOT aligns with the hydration of the polymer matrix, causing expansion and confirming the hydrogel formation. This hydration process supports the hypothesis that water molecules are integrated within the polymer network, resulting in a more voluminous hydrated structure [29].

Static water contact angle measurements also confirmed the hydration of PEDOT [21]. The measurements were conducted using the sessile drop method, where a 50 μL water droplet was carefully placed on each surface and imaged using a high-resolution digital camera. The results (Fig. S4 in the Supplementary material and carried out in triplicate) showed significant differences between the three surfaces. The unmodified electrode displayed a contact angle of (60.9 ± 0.4) °, indicative of moderate hydrophilicity of the underlying carbon material. PEDOT/AuNPs/SPCEs exhibited a slightly higher contact angle of (66.0 ± 0.6) °, indicating more hydrophobic behavior attributed to the hydrophobic nature of PEDOT, which can reduce the exposure of hydrophilic sites [30].

Conversely, hPEDOT/AuNPs/SPCE showed a markedly lower contact angle of (37.9 ± 0.3) °, indicating a substantial increase in hydrophilicity. This result is consistent with the formation of a hydrogel structure, where a hydrated polymeric network retains water molecules, creating a water-rich interface. The hydrophilic functional groups and swelling effect of the hydrogel enhance the surface's affinity for water. These observations confirm the successful hydration of PEDOT and the transition to a hydrogel state, which is critical for applications requiring anti-fouling, biocompatible surfaces in aqueous or biological environments [31,32].

All the results obtained provide a comprehensive characterization of PEDOT/AuNPs and hPEDOT/AuNPs on SPCEs. The transition from PEDOT to hPEDOT is marked by enhanced hydrophilicity, increased layer thickness, and greater surface roughness, which are indicative of hydrated hydrogel formation.

3.2. *Engineering the multifunctional hybrid polymer-hydrogel nanocomposite for the determination of HE*

The advantages provided by hPEDOT/AuNPs-modified electrodes were evaluated by comparing their performance with other electrode surface modifications, including *p*-ABA grafting, AuNPs, PEDOT, PEDOT/AuNPs, hPEDOT, AuNPs/hPEDOT, and hPEDOT/AuNPs using commercially available AuNPs-modified electrodes (GNPSPCEs) (Fig. 4**a**).

For this purpose, different immunoplatforms were prepared on these electrode substrates (Fig. 4**a**) and their amperometric responses in the absence (B signals) and in the presence (T signals) of 1 ng mL^{-1} HE was compared (Fig. 4**b**).

The cAb/hPEDOT/AuNPs/SPCE immunoplatform (configuration 7 in Fig. 4**b**) provided markedly better recognition of the target protein compared to conventional immobilization strategies, including electrode functionalization via electrochemical grafting of *p*-ABA (configuration 1). Notably, the hPEDOT/AuNPs system reached almost double T/B ratio compared with *p*-ABA grafting (6.1 *vs.* 3.4), underscoring its enhanced biointerface properties. This superior performance likely stems from the molecular architecture of hPEDOT-based materials, which enable more efficient surface modification and biorecognition.

In contrast, when SPCEs were first modified with AuNPs (widely used in electrochemical biosensing), the surface conductivity was improved, but non-specific adsorptions (B signals, gray bars in Fig. 4**b**) also increased significantly (immunoplatforms 2 and 4). This heightened nonspecific interaction compromises the selectivity of the system, ultimately diminishing the reliability of the biotarget detection.

The integration of hPEDOT demonstrates its ability to suppress nonspecific signals (configurations 3, 6, and 7) largely due to the hydrophilic nature of PEDOT, which fosters a hydrated interface that minimizes nonspecific adsorption. This aligns with previous studies [19] reporting the benefits of hPEDOT for enzymatic interfaces. A direct comparison between PEDOT (non-hydrated form, configuration 5) and hPEDOT (hydrated form, configuration 7) under identical conditions confirmed the superior performance of hPEDOT.

The results obtained also suggest that the order in which the AuNPs and hPEDOT are deposited (configurations 4 and 7) plays a determining role in the performance of the immunoplatform. As can be observed, when hPEDOT is electropolymerized onto a layer of electrodeposited

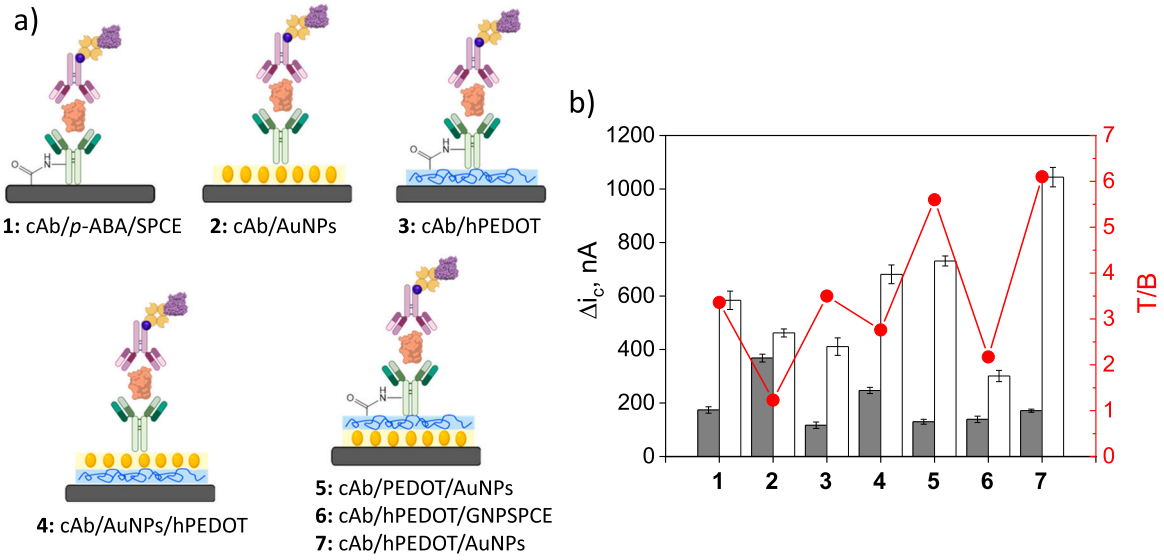

Fig. 4. a) Schematic representation of different immunosensing configurations evaluated. b) Evaluation of the recognition efficiency of the different immunoplatforms by comparing the amperometric responses they provided in the absence (B signals, gray bars) and in the presence (T signals, white bars) of 1 ng mL^{-1} HE and the resultant T/B ratio (red dots). a) Created in BioRender. Campuzano Ruiz, S. (2025) https://BioRender.com/har9d8o. Error bars in b) correspond to three times the standard deviation of replicates (n = 3).

AuNPs (configuration 7) there is a significant decrease in the B response and an increment in the T signal, resulting in a larger T/B ratio compared with the configuration where hPEDOT is electrodeposited first (6.1 *vs.* 2.8 for immunoplatforms 7 and 4, respectively). This synergistic interface amplifies recognition capabilities, leveraging AuNPs as a nanostructured scaffold to orchestrate and orient the hPEDOT polymer chains. Beyond conductivity, the highly organized interface formed over AuNPs supports selective binding interactions with the target biomolecule. The interplay between AuNPs nanostructural advantages and hPEDOT antifouling properties results in an optimized electrode surface with significantly improved sensitivity and specificity.

The critical role of controlled AuNPs electrodeposition becomes evident when comparing configurations 6 and 7 using electrodes commercially available with AuNPs or nanostructured in the laboratory, respectively. In this latter configuration, precise regulation over AuNPs size and density enabled the well-ordered deposition of hPEDOT, further refining sensitivity and selectivity.

A substantial enhancement in T/B ratio was found for the cAb/hPEDOT/AuNPs/SPCE immunoplatform (7) compared to that obtained with cAb/*p*-ABA/SPCE (1) and cAb/AuNPs/SPCE (2). Similarly, the strategic combination of hPEDOT with AuNPs further augmented T/B ratio, particularly when AuNPs are electrodeposited on SPCE and served as a molecular template to pre-organize monomers during EDOT electropolymerization. Interestingly, while the AuNPs/hPEDOT configuration (4) also exhibited improved T signal compared to hPEDOT configuration (3), probably due to the immobilization of cAb through direct chemisorption on AuNPs [5], its higher B signal suggests increased susceptibility to non-specific adsorptions. This trend was also observed for AuNPs alone (configuration 2).

Most notably, the hydrated form of the polymer outperforms its non-hydrated counterpart, both electropolymerized onto AuNPs. A direct comparison between configurations 5 and 7 reveals an enhancement in T/B, emphasizing the relevance of hydrating the polymer.

3.3. Refinement of experimental parameters

A comprehensive optimization of the experimental conditions involved in the preparation of the immunoplatform was carried out. All the evaluated variables (see Fig. S5) were selected according to the larger T/B ratio. The discussion of the optimization studies as well as a Table (Table S2), outlining each tested parameter along with the selected value, are provided in the Supplementary material.

The results of these optimizations confirm the important role of AuNPs, hPEDOT, and citrate (bars 0 in Figs. S5a-**c**) in the performance of the immunoplatform, as well as the rationale of the sandwich immunoassay (T/B ratio close to 1 in the absence of cAb, btn-DAb, and Strep-HRP, bars 0 in Figs. S5e, **k**, and **m**).

3.4. Analytical and operational characteristics

Under the optimized experimental conditions, the analytical and operational performance of the developed immunoplatform for the determination of HE was evaluated.

Fig. 5 shows the calibration plots and Table 2 the corresponding characteristic parameters obtained for the 7 immunoplatform configurations compared in Fig. 4. A linear correlation was observed between the amperometric signal and HE concentration for hPEDOT/AuNPs/SPCEs (configuration 7) within the 0.14 – 1 ng mL^{-1} range, showing a high sensitivity imparted by using the nanostructured material. In contrast, the calibration plot obtained with PEDOT/AuNPs/SPCEs (configuration 5) exhibited a lower slope, which underscores the role of hydration in enhancing the functionality of the polymer.

The results obtained with the other configurations tested agreed with the observations discussed in relation to Fig. 4. So, considerably lower slope values were obtained for calibration graphs constructed with cAb/*p*-ABA/SPCE and cAb/AuNPs/SPCE immunoplaforms (configurations 1 and 2). Moreover, a high intercept value was found when using immunoplatform 2, and it was confirmed that the arrangement of the AuNPs and the hPEDOT is a determining factor in the functioning of the immunoplatform (configurations 4 and 7). In addition, much better results were obtained when electrodepositing AuNPs on the SPCE in comparison with the commercially available electrodes with AuNPs (configurations 6 and 7). Also, the slope value of the immunoplatform incorporating hPEDOT on AuNPs was about 3-fold higher than that obtained with the configuration 3 which can be attributed to the increased population of immobilized cAb resulting in more HE binding [16].

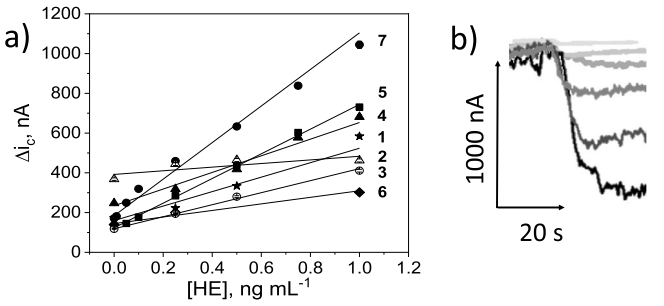

Fig. 5. a) Calibration curves for the determination of HE obtained with cAb/*p*-ABA/SPCE (**1,** stars); cAb/AuNPs/SPCE (**2**, open triangles); cAb/hPEDOT/SPCE (**3,** open circles); cAb/AuNPs/hPEDOT/SPCE (**4,** triangles); cAb/PEDOT/AuNPs/SPCE (**5,** squares); cAb/hPEDOT/GNPSPCEs (**6,** diamonds); and cAb/hPEDOT/AuNPs/SPCE (**7,** circles) immunoplatforms. b) Amperometric traces recorded with the developed cAb/hPEDOT/AuNPs/SPCE immunoplatform (configuration 7). Error bars in a) correspond to three times the standard deviation of replicates (n = 3).

Table 2
Parameters obtained from the calibration curves shown in Fig. 5**a**).

Configuration	Intercept, nA mL ng^{-1}	Slope, nA mL ng^{-1}	r^2
1: cAb/*p*-ABA/SPCE	144 ± 27	423 ± 47	0.976
2: cAb/AuNPs/SPCE	399 ± 27	82 ± 48	0.978
3: cAb/hPEDOT/SPCE	122 ± 7	294 ± 12	0.998
4: cAb/AuNPs/hPEDOT/SPCE	223 ± 21	450 ± 34	0.978
5: cAb/PEDOT/AuNPs/SPCE	90 ± 5	733 ± 32	0.996
6: cAb/hPEDOT/GNPSPCE	149 ± 13	156 ± 21	0.990
7: cAb/hPEDOT/AuNPs/SPCE	184 ± 10	920 ± 59	0.992

The detection (LOD) and quantification (LOQ) limits calculated using the cAb/hPEDOT/AuNPs/SPCE immunoplatform were estimated from the standard deviation of the blank (s_B) and the slope of the calibration curve. The obtained values were 0.04 ng mL^{-1} and 0.14 ng mL^{-1}, respectively. Importantly, these values are notably below the mean values reported in literature for HE levels in plasma from healthy individuals (43.2 ng mL^{-1}) and CRC patients (71.6 ng mL^{-1}) [33].

The reproducibility of the developed methodology was evaluated by measuring the amperometric signals obtained for 0.5 ng mL^{-1} HE with 10 different immunoplatforms prepared in the same manner, over several days. A relative standard deviation (RSD) of 3.5 % was found, thus indicating an excellent reproducibility and consistency of the immunoplatform fabrication and electrochemical measurement protocols.

Table S3 (in the Supplementary material) compares the analytical performance and key characteristics of the developed cAb/hPEDOT/AuNPs/SPCE immunoplatform with other available immunoassays/immunotechnology for the determination of HE detection. These are mostly ELISA type and only one electrochemical. The LOD achieved in

this work is comparable to values claimed for ELISA kits. However, these values are calculated mostly from non-linear logarithmic ranges and the precision levels are around 10 % or higher. Moreover, the criteria used to calculate the LOD values for these kits are rarely given in the commercial protocols. An important highlight of this work is the significantly shorter testing time required, a key advantage, especially for real-time or high-throughput applications, underscoring the potential of the immunoplatform for rapid and efficient HE determination. In addition, the amperometric immunoassay works with portable and cost-effective instrumentation which makes it more attractive for routine determinations in decentralized settings and implementation in point-of-care testing (POCT) devices. Recently our group has reported the only electrochemical immunoplatform described so far for the determination of this biomarker [14]. The method involved a sandwich format implemented on the surface of carboxyl-functionalized magnetic microbeads (MBs) and amperometric transduction at SPCEs using the HRP/H_2O_2/HQ system. Although there were no notable differences between the performance of the two electrochemical platforms in terms of analytical characteristics and assay time, the integrated immunoplatform described in this work exhibits advantages for potential point-of-need applications, where the incubators required for handling magnetic microparticles may be considered a disadvantage.

3.5. Evaluation of the immunoplatform selectivity

To check the selectivity of the developed HE immunoplatform, several non-target proteins, including common circulating human proteins such as hIgG, Hb, and HSA, as well as tumor-associated biomarkers such as TNFα, and IL13Rα2 [34–39], were tested at their typical concentrations in serum and plasma of healthy individuals.

Cross-reactivity studies were performed by comparing the amperometric signals provided by the immunoplatform for 0 and 1 ng mL^{-1} HE standards in the absence and in the presence of the potential interferent. As Fig. S6 (in the Supplementary material) shows, no significant changes in the T/B ratios were observed for any of the tested proteins, underscoring the high selectivity of the immunoplatform and supporting its reliability for applications in complex biological samples.

3.6. Immunoplatforms stability: hPEDOT/AuNPs/SPCE vs. PEDOT/AuNPs/SPCE

The long-term stability of the developed immunoplatform was evaluated by storage in a humid chamber in a refrigerator and recording the amperometric measurements both in the presence and in the absence of 1 ng mL^{-1} HE to assess potential degradation or loss of functionality over time (Fig. S7 in the Supplementary material). Fig. S7a shows the hPEDOT/AuNPs/SPCE immunoplatform allowed stable amperometric responses to be obtained over a period minimum of 30 days, indicating the hydrated polymer formulation retains its performance and reliability over time, crucial for long-term biosensing applications.

However, the PEDOT/AuNPs/SPCE immunoplatform showed under the same conditions noticeable fluctuations in the amperometric responses over time (Fig. S7b). These results highlight the benefits of using hPEDOT/AuNPs system in the development of more robust and stable immunoplatforms.

3.7. Evaluation of antifouling ability

The nanomaterial designed in this study, hPEDOT/AuNPs, was specifically engineered to exhibit antifouling properties, as the developed immunoplatform is intended for application in complex real samples [21]. Fouling, or the nonspecific adsorption of proteins, cells, and other biological samples components, can compromise sensor sensitivity and reproducibility by obstructing the electrode surface and altering the electrochemical signal [40]. Therefore, antifouling performance is essential to develop electrochemical biosensors with reliable functionality in challenging sample matrices. Antifouling properties of hPEDOT have been claimed in the literature [41]. This effect is attributed to the hydrated polymer layer, which repels nonspecific adsorptive interactions and the establishment of a water-based barrier that limits protein and cell adhesion.

To check such antifouling performance, immunoplatforms prepared with hPEDOT/AuNPs or non-hydrated PEDOT/AuNPs were incubated for 24 h after the blocking step in different media (PBS, serum, and urine) and their amperometric responses for 0 and 1 ng mL^{-1} HE compared with those obtained with non-incubated immunoplatforms. As illustrated results in Fig. 6 and data summarized in Table 3, cAb/hPEDOT/AuNPs/SPCE-immunoplatforms exhibited significantly improved antifouling behavior, providing responses with minimal current decrease. On the contrary, the immunoplatforms prepared with non-hydrated PEDOT (cAb/PEDOT/AuNPs/SPCE), showed a notable fouling with important signal drops. These results confirmed that polymer hydration enhances resistance to nonspecific adsorption, making hPEDOT/AuNPs an effective material for electrochemical sensing in biological fluids. This antifouling property not only enhances biosensor accuracy but also underscores hPEDOT's suitability for applications that require high sensitivity and durability in complex biological matrices.

3.8. Analysis of plasma samples

The developed cAb/hPEDOT/AuNPs/SPCE immunoplatform was employed to analyze (in triplicate) plasma samples from three distinct groups: healthy individuals (n = 3), individuals with premalignant lesions (n = 3), and patients diagnosed with CRC in early stage (CRC (I) n = 3).

To check a potential matrix effect, the slope of the calibration plot for HE obtained in buffer solution (slope: 920 ± 59 nA mL ng^{-1}) was statistically compared with the slope value for the calibration graph constructed from 200-fold diluted plasma samples from a healthy individual (slope: 892 ± 70 nA mL ng^{-1}). Statistical analysis showed no significant differences between both slope values with a t-exp value of 2.044, which was below the critical t-value of 2.353 (n = 5, α = 0.05). This indicates that no significant matrix effect occurred under the above-mentioned conditions. Thus, the concentrations of HE in the plasma samples were calculated by interpolating the measured signals into the calibration plot obtained with standard solutions (calibration plot 7 in Fig. 7**a**).

The results obtained for the plasma samples are summarized in

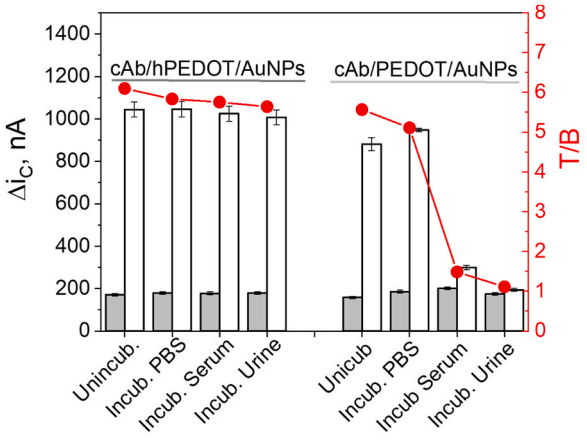

Fig. 6. Evaluation of cAb/hPEDOT/AuNPs/SPCE and cAb/PEDOT/AuNPs/SPCE immunoplatforms antifouling behavior. Comparison of the amperometric responses obtained with unincubated or 24 h incubated immunoplatforms in PBS, undiluted commercial human serum and urine, in the absence (grey, B) and in the presence of 1 ng mL^{-1} (white, T) of HE standard and the resulting T/B ratio (in red). Error bars correspond to three times the standard deviation of replicates (n = 3).

Table 3
Comparative table showing the % of T/B provided by each bioplatform after 24 h incubation in each medium.

% T/B provided by each bioplatform		
Condition	cAb/hPEDOT/AuNPs/ SPCE	cAb/PEDOT/AuNPs/ SPCE
PBS (t_0)	100	100
PBS (24 h inc.)	96	92
Undiluted serum (24 h inc.)	94	27
Undiluted urine (24 h inc.)	93	20

Fig. 7**a**, where the average concentrations of HE in healthy individuals, patients with premalignant lesions, and CRC patients are compared.

The obtained results revealed an increase in the plasma concentration of HE in parallel with the progression of the disease, with HE plasma levels higher in individuals with premalignant lesions and/or CRC patients in comparison with healthy individuals. This pronounced increase from healthy individuals to CRC patients strongly suggests that HE can serve as a crucial biomarker for testing the disease progression, where its early detection may significantly enhance patient survival prospects.

Additionally, the diagnostic capacity of the developed immunoplatform for HE in individuals with premalignant lesions and/or CRC patients was evaluated by ROC curve analysis (Fig. 7**b**). Optimal cut-off values of 63.6 ng mL^{-1} and 93.6 ng mL^{-1} were calculated to distinguish individuals with premalignant lesions and CRC patients from healthy individuals, respectively, with a full discrimination ability (100 % sensitivity, specificity, and area under the curve (AUC)) in both cases. Furthermore, the HE plasma levels allow also to distinguish between individuals with premalignant lesions and CRC patients (cut-off 122.63 ng mL^{-1}) with a 100 % sensitivity and specificity. These findings underscore the potential of HE as a biomarker for early CRC detection and highlight the applicability of the immunoplatform for clinical diagnostics.

It is important to remark that the results obtained in the analysis of plasma samples agreed with those reported by other authors who established cut-off values of 172 ng mL^{-1} in serum of CRC patients [15] and 67.8 ng mL^{-1} in plasma to discriminate healthy individuals and patients with CRC I [14].

Moreover, the accuracy of the developed immunoplatform for the analysis of plasma samples was evaluated through recovery experiments. Plasma samples of each group (healthy, premalignant lesions, and CRC (I)) were supplemented with a known concentration of HE standard to assess the immunoplatform performance in the presence of both endogenous and supplemented biotarget. Following the same procedure used for non-supplemented samples, the measured concentration post-spiking was corrected by subtracting the endogenous content, allowing for the determination of recovery efficiency. The recovery values, shown in Table S4 (in the Supplementary material), range from 99 % to 100 %. These results further validate the robustness of the methodology and its suitability for reliable quantification of HE in plasma samples.

4. Conclusions

This work reports the successful design and application of a novel and multifunctional nanostructured electrode modifier using hydrated

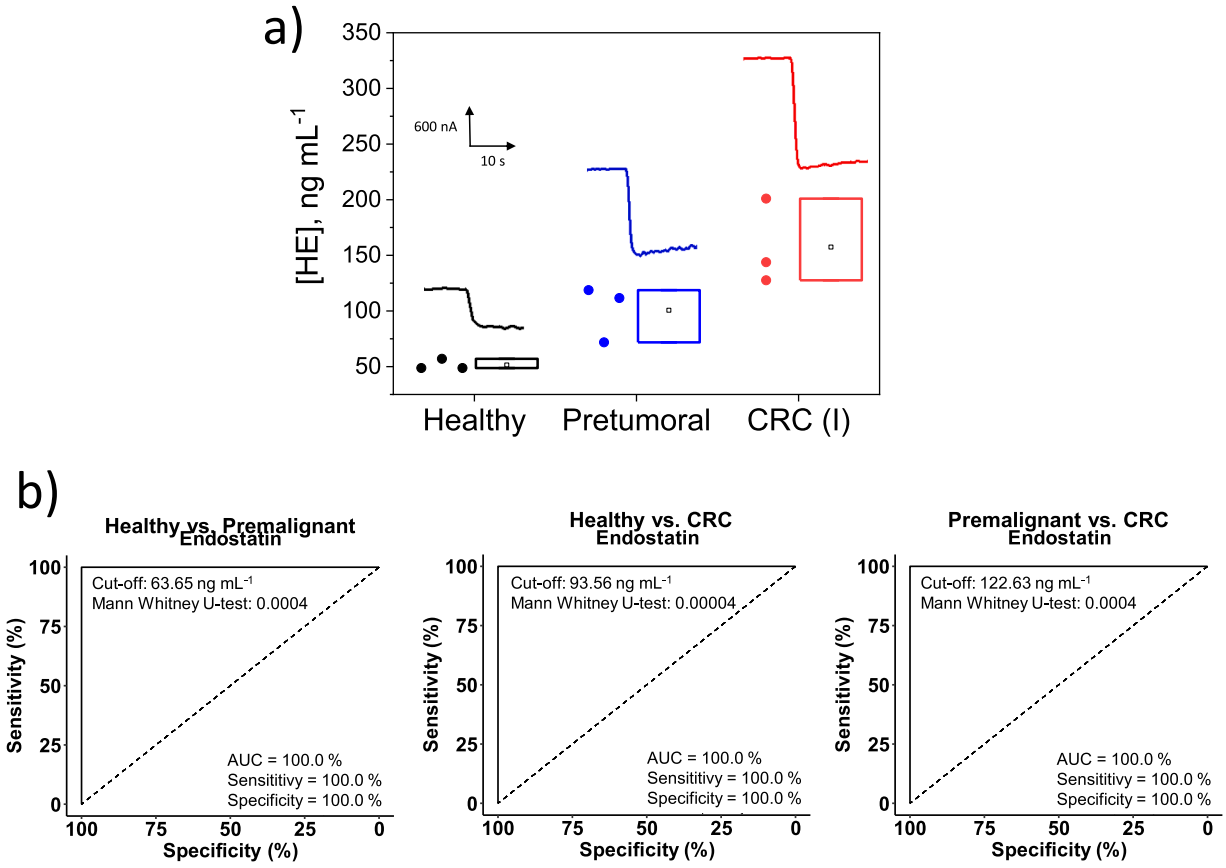

Fig. 7. a) HE concentrations in plasma of healthy individuals (black), individuals with premalignant lesions (blue), and CRC patients at stage I (red). Representative amperograms of each type of sample analyzed are shown. b) ROC curve analysis of the results obtained depicting the diagnostic potential for the discrimination of healthy individuals from premalignant or CRC patients, or premalignant from CRC patients. The cut-off value (threshold) for the indicated discrimination is shown in the inset of each individual ROC curve.

PEDOT (hPEDOT) in combination with AuNPs to be employed in electrochemical immunosensing. The engineered hPEDOT/AuNPs material provides a highly conductive, hydrophilic, and biocompatible interface with antifouling properties and an increased electroactive surface area, which are essential characteristics for applications in complex biological matrices. These unique features enabled the stable covalent immobilization of antibodies and efficient electron transfer, leading to improved sensitivity and selectivity.

Implemented on SPCEs, the developed sandwich-type amperometric immunoplatform enabled the sensitive and specific detection of HE, a biomarker of interest in CRC, with a low LOD (0.04 ng mL^{-1}), broad linear range, and excellent operational stability and reproducibility. Compared to conventional enzymatic labeling and ELISA-based formats, the proposed system offers faster analysis, reduced reagent consumption, and compatibility with low-cost, portable electrochemical instrumentation, making it highly promising for decentralized diagnostics and POCT. Furthermore, the exhaustive comparison of different immunosensing configurations clearly highlights the relevance of the nanocomposite components, their arrangement and polymer hydration in the functioning of the immunoplatform, mainly in terms of sensitivity, stability, and anti-fouling properties.

Importantly, the analysis of plasma samples validated the platform's capability to significantly distinguish between healthy individuals, individuals with premalignant lesions, and CRC patients at stage I as assessed by ROC curve analyses, not only reinforcing the diagnostic potential of HE in early disease detection but also demonstrating the usefulness of the developed immunoplatform. Indeed, the successful integration of hPEDOT and AuNPs within a hybrid material platform opens new possibilities not only for immunosensing but also for broader affinity-based biosensing strategies and transduction modes in particularly complex samples leveraging the attractive antifouling properties demonstrated by the multifunctional hybrid polymer-hydrogel nanocomposite engineered.

CRediT authorship contribution statement

Dilek Eskiköy Bayraktepe: Writing – review & editing, Resources. **Zehra Yazan:** Writing – review & editing, Resources. **Ana Montero-Calle:** Writing – review & editing, Resources. **Verónica Serafín:** Writing – original draft, Supervision, Methodology, Investigation, Data curation. **Susana Campuzano:** Writing – original draft, Supervision, Resources, Funding acquisition, Conceptualization. **Rodrigo Barderas:** Writing – review & editing, Resources, Funding acquisition. **José M. Pingarrón:** Writing – review & editing, Resources. **María Pedrero:** Writing – original draft, Supervision. **Ceren Yildiz:** Writing – review & editing, Methodology, Investigation. **Sara Santiago:** Writing – original draft, Supervision, Methodology, Investigation. **Andrea Cabrero-Martín:** Writing – original draft, Methodology, Investigation, Data curation.

Human ethics and consent to participate declarations

The plasma samples from healthy and CRC patients handled and analyzed were provided by the biobank of Hospital Clínico San Carlos after approval of the corresponding Ethical Committee (CEI PI 13_2020-v2 and CEI PI 90_2023). Written informed consent was obtained from all study participants.

Clinical trial number

Not applicable.

Declaration of Competing Interest

The authors declare that they have no known competing financial interests or personal relationships that could have appeared to influence the work reported in this paper.

Acknowledgement

The financial support of Grants PID2022–136351OB-I00 and PID2022–140307OB-I00 funded by MCIN/AEI/10.13039/501100011033 and by "ERDF A way of making Europe" to S.C. and R.B. respectively, and PI20CIII/00019 and PI23CIII/00027 grants from the AES-ISCIII program to R.B. are gratefully acknowledged. A.C-M. acknowledges a predoctoral contract (PREP2022–000170) and S.S. a Juan de la Cierva contract (JDC2022–048757-I) both from the Spanish Ministerio de Ciencia e Innovación. The technical assistance of the staff of the National Centre for Electron Microscopy (ICTS-CNME, Complutense University of Madrid) is also greatly appreciated.

Appendix A. Supporting information

Supplementary data associated with this article can be found in the online version at doi:10.1016/j.snb.2025.138480.

Data Availability

Data will be made available on request. The authors confirm that the data supporting the findings of this study are available within the article and its supplementary materials.

References

[1] A.S. Bhattacharyya, Conducting polymers in biosensing: a review, Chem. Phys. Impact 8 (2024) 100642, https://doi.org/10.1016/j.chphi.2024.100642.
[2] J.A. Janardhanan, H. Yu, Recent advances in PEDOT/PProDOT-derived nano biosensors: engineering nano assemblies for fostering advanced detection platforms for biomolecule detection, Nanoscale 16 (2024) 17202, https://doi.org/10.1039/D4NR01449A.
[3] B.M. Kangarshahi, S. Sojdeh, H. Daneshgar, M. Bagherzadeh, S.M. Naghib, N. Rabiee, Electroconductive polymer-based biosensors for early cancer detection via liquid biopsy: advances, challenges, and future prospects, TrAC Trends Anal. Chem. 183 (2025) 118062, https://doi.org/10.1016/j.trac.2024.118062.
[4] A. John, L. Benny, A.R. Cherian, S. Narahari, Y. Varghese, A.G. Hegde, Electrochemical sensors using conducting polymer/noble metal nanoparticle nanocomposites for the detection of various analytes: a review, J. Nanostruct. Chem. 11 (2021) 1–31, https://doi.org/10.1007/s40097-020-00372-8.
[5] J. Choosang, S. Khumngern, N. Nontipichet, P. Thavarungkul, P. Kanatharana, A. Numnuam, 3D porous CS-AuNPs-PEDOT-PB nanocomposite cryogel for highly sensitive label-free electrochemical immunosensor for carcinoembryonic antigen determination, Microchem. J. 187 (2023) 108435, https://doi.org/10.1016/j.microc.2023.108435.
[6] T. Karasu, C. Armutcu, K. Elkhoury, E. Ozgür, A. Maziz, L. Uzun, Conducting polymers as a functional recognition interface to design sensors for pathogen and cancer diagnosis, TrAC Trends Anal. Chem. 175 (2024) 117705, https://doi.org/10.1016/j.trac.2024.117705.
[7] M.A. Bhat, R.A. Rather, A.H. Shalla, PEDOT and PEDOT:PSS conducting polymeric hydrogels: a report on their emerging applications, Synth. Met 273 (2021) 116709, https://doi.org/10.1016/j.synthmet.2021.116709.
[8] M. Kim, R. Lezzi Jr, B.S. Shim, D. C, Martin, impedimetric biosensors for detecting vascular endothelial growth factor (VEGF) based on poly(3,4-ethylene dioxythiophene) (PEDOT)/gold nanoparticle (Au NP) composites, Front. Chem. 7 (2019) 234, https://doi.org/10.3389/fchem.2019.00234.
[9] L. Meng, A.P.F. Turner, W.C. Mak, Modulating electrode kinetics for discrimination of dopamine by a PEDOT:COOH interface doped with negatively charged tricarboxylate, ACS Appl. Mater. Interfaces 11 (2019) 34497–34506, https://doi.org/10.1021/acsami.9b12946.
[10] Y. Hui, C. Bian, S. Xia, J. Tong, J. Wang, Synthesis and electrochemical sensing application of poly(3,4-ethylenedioxythiophene)-based materials: a review, Anal. Chim. Acta 1022 (2018) 1–19, https://doi.org/10.1016/j.aca.2018.02.080.
[11] Q. Xu, J. Xu, H. Jia, Q. Tian, P. Liu, S. Chen, Y. Cai, X. Lu, X. Duan, L. Lu, Hierarchical Ti_3C_2 MXene-derived sodium titanate nanoribbons/PEDOT for signal amplified electrochemical immunoassay of prostate specific antigen, J. Electroanal. Chem. 860 (2020) 113869, https://doi.org/10.1016/j.jelechem.2020.113869.
[12] M. Cui, Z. Song, Y. Wu, B. Guo, X. Fan, X. Luo, A highly sensitive biosensor for tumor marker alpha fetoprotein based on poly(ethylene glycol) doped conducting polymer PEDOT, Biosens. Bioelectron. 79 (2016) 736–741, https://doi.org/10.1016/j.bios.2016.01.012.
[13] G. Wang, R. Han, X. Su, Y. Li, G. Xu, X. Luo, Zwitterionic peptide anchored to conducting polymer PEDOT for the development of antifouling and ultrasensitive electrochemical DNA sensor, Biosens. Bioelectron. 92 (2017) 396–401, https://doi.org/10.1016/j.bios.2016.10.088.
[14] S. Tejerina-Miranda, M. Pedrero, M. Blázquez-García, V. Serafín, A. Montero-Calle, M. Garranzo-Asensio, A.J. Reviejo, J.M. Pingarrón, R. Barderas, S. Campuzano, Angiogenesis inhibitor or aggressiveness marker? The function of endostatin in

cancer through electrochemical biosensing, Bioelectrochemistry 155 (2024) 108571, https://doi.org/10.1016/j.bioelechem.2023.108571.
[15] T. Kantola, J.P. Väyrynen, K. Klintrup, J. Mäkelä, S.M. Karppinen, T. Pihlajaniemi, H. Autio-Harmainen, T.J. Karttunen, A. Tuomisto, Serum endostatin levels are elevated in colorectal cancer and correlate with invasion and systemic inflammatory markers, Br. J. Cancer 111 (2014) 1605–1613, https://doi.org/10.1038/bjc.2014.456.
[16] J. Choosang, P. Thavarungkul, P. Kanatharana, A. Numnuam, AuNPs/PpPD/PEDOT:PSS-Fc modified screen-printed carbon electrode label-free immunosensor for sensitive and selective determination of human serum albumin, Microchem. J. 155 (2020) 104709, https://doi.org/10.1016/j.microc.2020.104709.
[17] A.L. Lorenzen, A.M. Dos Santos, L.P. Dos Santos, L. da Silva Pinto, F.R. Conceição, F. Wolfart, PEDOT-AuNPs-based impedimetric immunosensor for the detection of SARS-CoV-2 antibodies, Electrochim. Acta 404 (2022) 139757, https://doi.org/10.1016/j.electacta.2021.139757.
[18] V.Carralero Sanz, Preparación de biosensores enzimáticos e inmunosensores basados en electrodos modificados con nanopartículas de oro, Doctoral Thesis, Universidad Complutense de Madrid, Madrid, 2009. ⟨https://hdl.handle.net/20.500.14352/48708⟩.
[19] K. Promsuwan, L. Meng, P. Suklim, W. Limbut, P. Thavarungkul, P. Kanatharana, W.C. Mak, Bio-PEDOT: modulating carboxyl moieties in poly(3,4-ethylenedioxythiophene) for enzyme-coupled bioelectronic interfaces, ACS Appl. Mater. Interfaces 12 (2020) 39841–39849, https://doi.org/10.1021/acsami.0c10270.
[20] B. Yao, H. Wang, Q. Zhou, M. Wu, M. Zhang, C. Li, G. Shi, Ultrahigh-conductivity polymer hydrogels with arbitrary structures, Adv. Mater. 29 (2017) 1700974, https://doi.org/10.1002/adma.201700974.
[21] W. Wang, R. Han, M. Chen, X. Luo, Antifouling peptide hydrogel based electrochemical biosensors for highly sensitive detection of cancer biomarker HER2 in human serum, Anal. Chem. 93 (2021) 7355–7361, https://doi.org/10.1021/acs.analchem.1c01350.
[22] G. Martínez-García, L. Agüí, P. Yáñez-Sedeño, J.M. Pingarrón, Multiplexed electrochemical immunosensing of obesity-related hormones at grafted graphene-modified electrodes, Electrochim. Acta 202 (2016) 209–215, https://doi.org/10.1016/j.electacta.2016.03.140.
[23] B. Arévalo, M. Blázquez-García, A. Valverde, V. Serafín, A. Montero-Calle, G. Solís-Fernández, R. Barderas, S. Campuzano, P. Yáñez-Sedeño, J.M. Pingarrón, Binary MoS_2 nanostructures as nanocarriers for amplification in multiplexed electrochemical immunosensing: simultaneous determination of b cell activation factor and proliferation-induced signal immunity-related cytokines, Microchim. Acta 189 (2022) 1–15, https://doi.org/10.1007/S00604-022-05250-4.
[24] J.M. Pingarrón, & P. Yáñez-Sedeño. Química electroanalítica: Fundamentos y aplicaciones. Ed. Síntesis. (1999).
[25] V. Serafín, R.M. Torrente-Rodríguez, A. González-Cortés, P. García de Frutos, M. Sabaté, S. Campuzano, P. Yáñez-Sedeño, J.M. Pingarrón, An electrochemical immunosensor for brain natriuretic peptide prepared with screen-printed carbon electrodes nanostructured with gold nanoparticles grafted through aryl diazonium salt chemistry, Talanta 179 (2018) 131–138, https://doi.org/10.1016/j.talanta.2017.10.063.
[26] A.E. Deller, B.M. Hryniewicz, C. Pesqueira, R.P. Horta, B.J.G. da Silva, S. Weheabby, A. Al-Hamry, O. Kanoun, M. Vidotti, PEDOT:PSS/AuNPs-based composite as voltammetric sensor for the detection of pirimicarb, Polymers 15 (2023) 739, https://doi.org/10.3390/POLYM15030739.
[27] W. Cheng, Y. Liu, Z. Tong, Y. Zhu, K. Cao, W. Chen, D. Zhao, H. Yu, Micro-interfacial polymerization of porous PEDOT for printable electronic devices, EcoMat 5 (2023) e12288, https://doi.org/10.1002/eom2.12288.
[28] P. Lu, D. Ruan, M. Huang, M. Tian, K. Zhu, Z. Gan, Z. Xiao, Harnessing the potential of hydrogels for advanced therapeutic applications: current achievements and future directions, Signal Transduct. Target. Ther. 9 (2024) 1–66, https://doi.org/10.1038/s41392-024-01852-x.
[29] F.R. Ortega, G. Rodríguez, M.R. Aguilar, J. García-Sanmartín, A. Martínez, J. San Román, F.R. Ortega, Comportamiento reológico de geles biodegradables para aplicaciones en medicina regenerativa, Biomecánica 20 (2012) 7–19, https://doi.org/10.5821/sibb.v20i1.4664.
[30] H.J. Butt, J. Liu, K. Koynov, B. Straub, C. Hinduja, I. Roismann, R. Berger, X. Li, D. Vollmer, W. Steffen, M. Kappl, Contact angle hysteresis, Curr. Opin. Colloid Interface Sci. 59 (2022) 101574, https://doi.org/10.1016/J.COCIS.2022.101574.
[31] D.Y. Kwok, A.W. Neumann, Contact angle measurement and contact angle interpretation, Adv. Colloid Interface Sci. 81 (1999) 167–249, https://doi.org/10.1016/S0001-8686(98)00087-6.
[32] M. Rezaei, D.M. Warsinger, J.H. Lienhard V, M.C. Duke, T. Matsuura, W. M. Samhaber, Wetting phenomena in membrane distillation: mechanisms, reversal, and prevention, Water Res 139 (2018) 329–352, https://doi.org/10.1016/j.watres.2018.03.058.
[33] A.L. Feldman, H.R. Alexander, D.L. Bartlett, K.C. Kranda, M.S. Miller, N. G. Costouros, P.L. Choyke, S.K. Libutti, A prospective analysis of plasma endostatin levels in colorectal cancer patients with liver metastases, Ann. Surg. Oncol. 8 (2001) 741–745, https://doi.org/10.1007/s10434-001-0741-x.
[34] Q.W. Ben, Z. Zhao, S.F. Ge, J. Zhou, F. Yuan, Y.Z. Yuan, Circulating levels of periostin May help identify patients with more aggressive colorectal cancer, Int. J. Oncol. 34 (2009) 821–828, https://doi.org/10.3892/IJO_00000208.
[35] R. Barderas, R.A. Bartolomé, M.J. Fernandez-Aceñero, S. Torres, J.I. Casal, High expression of IL-13 receptor α2 in colorectal cancer is associated with invasion, liver metastasis, and poor prognosis, Cancer Res. 72 (2012) 2780–2790, https://doi.org/10.1158/0008-5472.CAN-11-4090.
[36] O.A. Al Obeed, K.A. Alkhayal, A. Al Sheikh, A.M. Zubaidi, M.A. Vaali-Mohammed, R. Boushey, J.H. Mckerrow, M.H. Abdulla, Increased expression of tumor necrosis factor-α is associated with advanced colorectal cancer stages, World J. Gastroenterol. 20 (2014) 18390–18396, https://doi.org/10.3748/wjg.v20.i48.18390.
[37] Z. Li, X. Zhang, Y. Yang, S. Yang, Z. Dong, L. Du, L. Wang, C. Wang, Periostin expression and its prognostic value for colorectal cancer, Int. J. Mol. Sci. 16 (2015) 12108, https://doi.org/10.3390/IJMS160612108.
[38] X. Deng, S. Ao, J. Hou, Z. Li, Y. Lei, G. Lyu, Prognostic significance of periostin in colorectal cancer, Chin. J. Cancer Res. 31 (2019) 547, https://doi.org/10.21147/J.ISSN.1000-9604.2019.03.16.
[39] F. Warsinggih, I. Limanu, R.E. Labeda, M. Lusikooy, M. Mappincara, Faruk, The relationship of tumor necrosis factor alpha levels in plasma toward the stage and differentiation degree in colorectal cancer, Med. Cl. íN. Pr. áct. 4 (2021) 100224, https://doi.org/10.1016/j.mcpsp.2021.100224.
[40] S. Saxena, P. Sen, L. Soleymani, T. Hoare, Anti-fouling polymer or peptide-modified electrochemical biosensors for improved biosensing in complex media, Adv. Sens. Res. 3 (2024) 2300170, https://doi.org/10.1002/adsr.202300170.
[41] G. He, W. Liu, Y. Liu, S. Wei, Y. Yue, L. Dong, L. Yu, Antifouling hydrogel with different mechanisms: antifouling mechanisms, materials, preparations and applications, Adv. Colloid Interface Sci. 335 (2025) 103359, https://doi.org/10.1016/J.CIS.2024.103359.

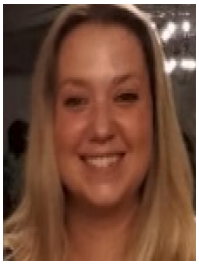

Verónica Serafín (ORCID: 0000–0003–0034–8456) has been an Assistant Professor in the Department of Analytical Chemistry at the Faculty of Chemical Sciences, Complutense University of Madrid, since 2020. She is a member of the Research Group "Electroanalysis and Electrochemical (Bio)sensors" (GEBE-UCM). Her current research focuses on the development of electrochemical biosensors based on the integration of cutting-edge multifunctional nanomaterials, which significantly enhance their analytical performance in terms of sensitivity, selectivity, and reliability. These biosensors are designed for the detection of candidate biomarkers relevant to the clinical and food sectors, with the aim of advancing diagnostics and ensuring food quality and safety.

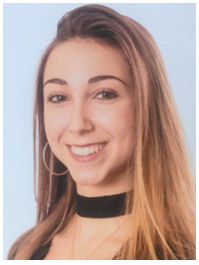

Andrea Cabrero-Martín (ORCID: 0009–0001–0785–1495) is a PhD candidate at the Faculty of Chemistry of the Complutense University of Madrid and has been a member of the Electroanalysis and Electrochemical (Bio)Sensors Research Group (GEBE-UCM) since 2024. Her research focuses equally on two main areas: the development of electrochemical biosensors based on epigenetic markers for the detection of cancer biomarkers in clinically relevant biological samples, aiming to enable point-of-care diagnostics for early cancer detection; and the design of nanostructured electrodes for electrochemical biosensors and immunosensors for the detection of clinically relevant analytes in the field of proteomics.

Sara Santiago (ORCID: 0000–0002–1206–1455) holds a Juan de la Cierva postdoctoral fellowship at the Department of Analytical Chemistry of the Faculty of Chemical Sciences at the Complutense University of Madrid. She is member of the "Electroanalysis and Electrochemical (Bio)sensors" Research Group (GEBE-UCM). Her work focuses on the development of cutting-edge electroanalytical bioplatforms for sustainable, equitable, and personalized medicine and nutrition. Her interests include colorimetric (bio)sensing, electrochromic devices, and self-powered wearables. She is currently involved in projects related to advanced (bio)sensor development at the point-of-care.

Ceren Yildiz (ORCID: 0009–0005–2927–0527) holds an MSc degree from the Department of Chemistry at Ankara University, Ankara, Turkey, obtained in 2020. She is currently a Ph.D. student at the same university. Her research focuses on electrochemistry, electroanalytical chemistry, electrochemical sensors and nanosensors, DNA biosensors, electrochemical drug-DNA interactions, and electrochemical sensors for heavy metals. She has more than 15 research articles.

Dilek Eskiköy Bayraktepe (ORCID: 0000–0001–8592–6766) has a Ph.D. degree from Ankara University, Department of Chemistry (Division of Analytical Chemistry), Ankara, Turkey, in 2017. She has been working as an associate professor at the university since 2021. Her research focuses on electrochemistry, electroanalytical chemistry, electrochemical sensors (including nanosensors, immunosensors, and DNA biosensors), and the investigation of electrochemical drug-DNA interactions. She has more than 35 research articles.

María Pedrero (ORCID: 0000–0002–2047–396X**)** is Assistant Professor at the Department of Analytical Chemistry of the Faculty of Chemical Sciences at the Complutense University of Madrid since 2002. She is a member of the "Electroanalysis and Electrochemical (Bio)sensors" Research Group (GEBE-UCM). Her research area includes the development and study of electrochemical (bio)sensors for the determination of proteins and oligonucleotides as markers of cancer and cardiovascular and neurological diseases. She is co-author of 135 journal articles (103 research articles and 32 review articles) and 13 book chapters on Analytical Electrochemistry, Sensors and Biosensors in Analytical Chemistry.

José M. Pingarrón (ORCID: 0000–0003–2271–1383) is Full Professor of Analytical Chemistry, founder and current member of the group "Electroanalysis and electrochemical (bio) sensors" (GEBE-UCM) at the Complutense University of Madrid. His lines of research include the development of nanostructured electrochemical platforms (enzymatic sensors, immunosensors and genosensors) for the simple or multiplexed determination of relevant biomarkers. He is an honorary advisory member of the journal Electroanalysis and since 2017 a "Fellow" of the International Society of Electrochemistry.

Ana Montero Calle is a post-doctoral research at the Functional Proteomics Unit of the Instituto de Salud Carlos III where she works investigating about early cognitive impairment and colorectal cancer by proteomics. She got her PhD at the Complutense University of Madrid in 2023, which was focused on the identification of new biomarkers for the diagnosis and prognosis of chronic diseases of high prevalence, including colorectal cancer and Alzheimer's disease, using different proteomics approaches. She has co-author more than 60 articles since 2017 and participated in more than 90 international and national congresses.

Rodrigo Barderas works as Tenured Scientist at the Instituto de Salud Carlos III. He is currently the Head of the Functional Proteomics Unit of the Chronic Disease Programme, and responsible for the proteomics facility at the Instituto de Salud Carlos III. His areas of interest include the identification of diagnostic and prognostic markers and new targets of intervention in chronic diseases of high prevalence by using proteomics and their translation to bioplatforms for precision healthcare, with a special focus on colorectal cancer. He has co-authored more than 150 scientific articles in international peer-review journals.

Zehra Yazan (ORCID: 0000–0002–7511–7508) obtained her Ph.D. from Ankara University, Faculty of Science, Department of Chemistry, Division of Analytical Chemistry in Turkey. Currently, she has been working as a full professor in the Chemistry Department in the Science Faculty at Ankara University since 2010. Her research focuses on electrochemistry, electroanalytical chemistry, electrochemical sensors (including nanosensors, immunosensors, and DNA biosensors), and the investigation of electrochemical drug-DNA interactions. She has more than 60 research articles.

Susana Campuzano (ORCID: 0000–0002–9928–6613) is Full Professor in the Department of Analytical Chemistry at the Faculty of Chemistry of the Complutense University of Madrid (Spain) and Director of the Research Group "Electroanalysis and Electrochemical (Bio)Sensors" (GEBE-UCM). Her areas of interest include the development of affinity-based electroanalytical biotechnologies with potential for multiplexed and/or multi-omic determinations in precision healthcare. She is an associate editor of the journal Electroanalysis (Wiley-VCH).